Using the nonlinear Breit-Wheeler process to test nonlinear vacuum birefringence

O. Borysov,[1,2] B. Heinemann,[2,3] A. Ilderton,[4] B. King,[2,5,*] and A. Potylitsyn[2]

[1]*Weizmann Institute of Science, 234 Herzl Street, Rehovot, 7610001 Israel*
[2]*Deutsches Elektronen-Synchrotron DESY, Notkestrasse 85, 22607 Hamburg, Germany*
[3]*Albert-Ludwigs-Universität Freiburg, 79104 Freiburg, Germany*
[4]*Higgs Centre, School of Physics and Astronomy, University of Edinburgh, Edinburgh, EH9 3HJ United Kingdom*
[5]*Centre for Mathematical Sciences, University of Plymouth, Plymouth PL4 8AA, United Kingdom*

(Received 3 October 2022; accepted 1 December 2022; published 23 December 2022)

Quantum electrodynamics predicts that the quantum vacuum is birefringent, but due to the very small cross-section this is yet to be confirmed by experiment. Vacuum birefringence arises as the elastic part of photon-photon scattering; the inelastic part is Breit-Wheeler pair production. We outline how measurements of the photon-polarized nonlinear Breit-Wheeler process can be used to infer a measurement of all-order, *nonlinear* vacuum birefringence. As an example scenario, we calculate the accuracy of such a measurement for parameters anticipated at upcoming laser-particle experiments.

DOI: 10.1103/PhysRevD.106.116015

I. INTRODUCTION

The quantum vacuum, exposed to strong electromagnetic fields, can behave as a refractive medium. The propagation of probe photons then becomes polarization-dependent, a phenomenon named vacuum birefringence. Here "vacuum" emphasizes that it is *virtual* electron-positron pairs which affect birefringence, as opposed to distributions of real matter in e.g. optics. Vacuum birefringence is a manifestion of *polarized* photon-photon scattering first predicted in the 1930s [1], but remaining unobserved. *Linear, unpolarised* scattering has been observed in ultraperipheral heavy-ion collisions at ATLAS [2,3] and CMS [4], and higher-order effects observed in unpolarized Delbrück scattering [5,6]. There have been many suggestions for how to measure polarized scattering via collisions of intense laser pulses [7,8], and for how to measure vacuum birefringence using X-ray photons to probe intense optical lasers [9,10], which is the focus of the planned HIBEF experiment [11]. Such experiments require sensitive X-ray polarimetry and face a significant challenge in separating signal from background. Suggestions for how to counter this, using e.g. shaped beams [12], has seen much attention in recent years. At similar field strengths but higher photon energies, vacuum birefringence becomes *nonlinear*, including all orders of interaction between the virtual pair and the intense background. Although there are suggestions for how to measure this directly [13–15], direct approaches must also address the difficulty of measuring the polarization of high-energy photons.

Here we propose a way to overcome these challenges and measure vacuum birefringence indirectly, via experiments on the, at first sight, very different process of pair production from polarized photons colliding with an intense laser, or "nonlinear Breit-Wheeler" (NBW) [16]. NBW is the target of several upcoming experiments [17,18]; the unpolarized process has so far only been observed in the E144 experiment [19,20] as part of the two-step trident process, while the polarised *linear* process was recently measured by the STAR Collaboration in ultraperipheral heavy-ion collisions [21]. (See also [22,23] for discussions of vacuum birefringence in the emissions of strongly magnetized neutron stars.) Specifically, we will show how the (already planned) LUXE experiment [17] can be simply modified to provide an indirect measurement of all-order, nonlinear vacuum birefringence i.e. probing photon-photon scattering beyond the linear regime previously investigated [21]. As we will see, this can be achieved by swapping the planned amorphous bremsstrahlung target with a diamond crystal radiator target to produce coherent bremsstrahlung (CB) as the source of photons (as has been demonstrated at similar photon energies in e.g. GlueX [24]).

Our proposal exploits two fundamental properties of quantum field theory. First, unitarity (the optical theorem)

*b.king@plymouth.ac.uk

relates the number of produced pairs to the imaginary part of the photon forward scattering amplitude. Second, analyticity (Kramers-Kronig relations, routinely used in nonlinear optics [25]) dictates the real part of the amplitude given the imaginary part. Thus, as we make precise below, a measurement of pair yield in polarized NBW implies a measurement of polarized photon-photon scattering, and thereby nonlinear vacuum birefringence. There are several advantages of such a scheme over matterless vacuum birefringence experiments; in high-energy laser-particle experiments, the pair production cross-section is orders of magnitude larger than that for elastic photon-photon scattering, and positrons are easier to measure than photons within a photon background, circumventing the "signal/noise" problem.

II. THEORY

Consider the collision of a high-energy photon and an intense laser pulse. The probability of pair creation by the photon is related, via the optical theorem, to the imaginary part of the photon forward scattering amplitude. Working to leading order in the fine-structure constant, α, but treating the interaction with the intense laser exactly, the optical theorem can be expressed as

$$2\,\mathrm{Im}$$  (1)

in which j represents the state of the photon and the double line represents "dressed" electrons/positrons interacting with the intense laser. Now, for every complex function $F(z)$ (analytic in the upper-half z-plane and vanishing faster than $1/|z|$ as $|z| \to \infty$) its real F^r and imaginary F^i parts are related by $F^r(z) = \mathcal{H}[F^i; z]$ in which $\mathcal{H}[F^i; z] = \pi^{-1}\mathrm{PV}\int \mathrm{d}z' F^i(z')/(z' - z)$ is the Hilbert transform. Thus, if z represents some appropriate variable in the NBW probability, then the transform w.r.t. z gives the real part of the photon forward scattering amplitude as, schematically

$$2\,\mathrm{Re}$$ 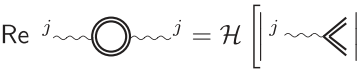 (2)

Combining (1) and (2), we obtain the full one-loop amplitude from tree-level NBW. This is related to work by Toll [26], who applied Kramers-Kronig to the vacuum "refractive indices" (see below); however, we need to extend these formal ideas to make them experimentally relevant. In particular we need to identify suitable F and z, and we need to know how to perform the Hilbert transformation in z given some experimental data on F. To achieve this we exploit the behavior of physical observables in the parameter regime of interest.

To produce a detectable number of pairs via NBW, one ideally requires the strong-field parameter of the photon χ, to satisfy $\chi \gtrsim 1$ where $\chi = |e|\sqrt{-(k\cdot\mathcal{F})^2}/m^3$ (m and $e < 0$ are the electron mass and charge, k is the photon momentum, $\mathcal{F}_{\mu\nu}$ the Faraday tensor of the laser and we set $\hbar = c = 1$). We also work in the intensity regime for which the locally constant field approximation applies [27,28]—this means the NBW probability in a focused laser pulse can be obtained by integrating a local rate, calculated in a constant crossed field, with the pulse profile [29,30]. This requires that the laser intensity parameter ξ satisfies $\xi \gg 1$ where $\xi \coloneqq \chi/\eta$ and $\eta = k\cdot\varkappa/m^2$ with $\varkappa$ the characteristic wavevector of the laser. In this regime, the polarized NBW rate depends nontrivially only on the strong-field parameter χ: our goal therefore is to apply the Hilbert transform in χ. (Indeed it has been shown that NBW at small χ can be Hilbert transformed to yield a resummation of the small-χ expansion of the real part of the vacuum refractive index [31].)

Now, let $\mathcal{M}_{ij}$ be the amplitude for a photon to scatter from polarization state $|i\rangle$ to $|j\rangle$. If $j = 1, 2$ represent a basis of linear polarizations transverse to the laser propagation direction, then the optical theorem relates the amplitudes $\mathcal{M}_{jj}$ to the probability P_j of NBW from a photon in polarization state $|j\rangle$. Furthermore in the regime of interest the helicity flip amplitude $\mathcal{M}_{+-}$ (where $|\pm\rangle = (|1\rangle \pm i|2\rangle)/\sqrt{2}$) obeys

$$2\mathcal{M}_{+-} = \mathcal{M}_{11} - \mathcal{M}_{22} \tag{3}$$

since $|1\rangle$ and $|2\rangle$ are polarization eigenstates and $\mathcal{M}_{12} = \mathcal{M}_{21} = 0$. Thus, the optical theorem applied to $\mathsf{P}_1 - \mathsf{P}_2$ is proportional to the imaginary part of $\mathcal{M}_{+-}$, while the Hilbert transform is proportional to the real part:

$$4\mathrm{Re}$$ 

Thus our Hilbert transform scheme gives access to "flip" and "no-flip" scattering amplitudes. (The kinematics of forward scattering yields a simple relationship between amplitudes and probabilities P_{ij} for the photon to change state from $|i\rangle$ to $|j\rangle$, namely $\mathsf{P}_{ij} = (\alpha/\eta)^2|\mathcal{M}_{ij}|^2$.)

III. TOWARD EXPERIMENT

Now, probe photon distributions in experiment are typically broadband, implying many different values of χ impact the pair yield. Therefore, the Hilbert transform will be over the maximum value of χ, which we denote χ_0 i.e. $\chi \in [0, \chi_0]$. We note in particular that it is generally easier to repeat the experiment at different χ_0 than at e.g. probe photon energy, because the former can be achieved simply by defocusing the laser, while the latter is determined by the photon source. Performing the Hilbert transform in χ_0 thus allows it to be evaluated with more experimental data

points, providing a more accurate inference of vacuum birefringence.

The optical theorem and Kramers-Kronig relations described above feature dressed propagators, including all orders of interaction between the field and the polarized virtual pair. This is easily made explicit: the scattering amplitude can be expanded in powers of (within the locally constant field approximation) χ^{2n} for $n \geq 1$, and successive terms correspond to vacuum polarization involving $2n$ photons from the background, as illustrated in Eq. (4). When $\chi \ll 1$, all orders of this interaction must be taken into account: in this regime vacuum polarization effects are *nonlinear*. This is to be contrasted with the weak-field Heisenberg-Euler result, corresponding to only the leading-order term of (4), which is insufficient to describe $\chi > 1$ vacuum polarization.

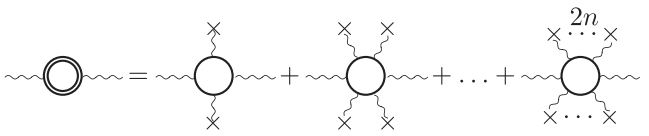

(4)

We now make these ideas precise, beginning with an estimate for the number of pairs N_j, produced when a distribution of photons, ρ_j, in polarization state $|j\rangle$, collides with a focused laser pulse. Treating the pulse as, locally, a plane wave, one integrates the plane wave NBW probability with the photon distribution, over the transverse structure of the pulse [32,33], which yields

$$N_j = \frac{2\alpha}{\eta} \int \mathrm{d}^2\mathbf{x}^\perp \int_0^1 \mathrm{d}s\ \rho_j(s) \int \mathrm{d}\varphi \frac{\partial \mathcal{M}^i_{jj}[\chi(\varphi)]}{\partial \varphi},$$

where $\mathbf{x}^\perp$ are the transverse coordinates, $\varphi = \varkappa \cdot x$ the laser phase, and $s \in [0,1]$ is the photon lightfront momentum fraction—the ratio of energies η/η_0, for η_0 the maximum value of η. (It is assumed that the photon distribution does not vary greatly over the focus of the laser pulse.) Finally, $\mathcal{M}^i_{jj}$ is the imaginary part of the photon forward scattering amplitude, which is, explicitly [34],

$$\frac{\partial \mathcal{M}_{jj}}{\partial \varphi} = \frac{2}{3} \int_4^\infty \frac{\mathrm{d}v}{i\pi} \frac{1}{z} \frac{v-4+3j}{v\sqrt{v(v-4)}} \int \mathrm{d}t\, t \mathrm{e}^{iz(\chi)t + it^3/3}, \quad (5)$$

for $j = 1, 2$ and where $z(\chi) = (v/\chi)^{2/3}$.

Writing $\chi_0 = \eta_0 \xi_0$, where ξ_0 is the maximum value of ξ, so that $\chi(s, \varphi, \mathbf{x}^\perp) = s\eta_0 \xi(\varphi, \mathbf{x}^\perp) = \chi_0 s f(\varphi, \mathbf{x}^\perp)$ (where f describes the spacetime dependence of the laser), we see that χ_0 is the single nontrivial input parameter for calculating the total number of pairs $N = N_1 + N_2$. To make this explicit, we define $F(\chi_0) = N/\eta_0 \xi_0^2$ which depends *solely* on χ_0. This is the function which we will Hilbert transform. (Note that this choice of F assists convergence of the numerical Hilbert transform as $F(\chi_0) \to 0$ quicker than $1/|\chi_0|$ as $\chi_0 \to \infty$.) Then suppose, for a range of χ_0 values, the number of pairs has been experimentally measured to produce a dataset for the pair yield, equivalently $F^i(\chi_0)$. This dataset is then linearly interpolated to acquire a curve $\mathcal{F}^i$, on which one can perform a numerical Hilbert transform to obtain the estimate $\overline{F^r}(\chi_0) := \mathcal{H}[\mathcal{F}^i; \chi_0]$ of the actual real part $F^r(\chi_0)$ of the elastic photon-scattering process. The accuracy of $\overline{F^r}(\chi_0)$ as an approximation to $F^r(\chi_0)$ naturally depends on how much of the curve $F^i(\chi)$ is known; this means the range of χ that F^i is measured over in experiment, as well as the accuracy of the individual measurements. We illustrate this with an idealized example before moving on to the actual setup of experimental interest.

Suppose the distribution of photons is monoenergetic and completely polarized in one state, and suppose the laser is modeled as a constant crossed field (a zero frequency plane wave). We construct the vacuum polarization F^r and pair yield F^i quantities in this setup. We pick a range of χ_0 starting at $\xi_0 = 2.5$ ($\chi_0 = 0.5$), within the region of validity of the locally constant field approximation [30] which we also use for our main results, below. A maximum value of $\chi_0 = 10$ is chosen. Performing the Hilbert transform of the pair data results in the approximation $\overline{F^r}$ to the vacuum polarization effect plotted in Fig. 1 (see Appendix A for details of this step). There is overall good agreement, even though the numerical Hilbert transform slightly underpredicts the true value of F^r. This is due to the fact that the parts of F^i lying outside the measured region are missing

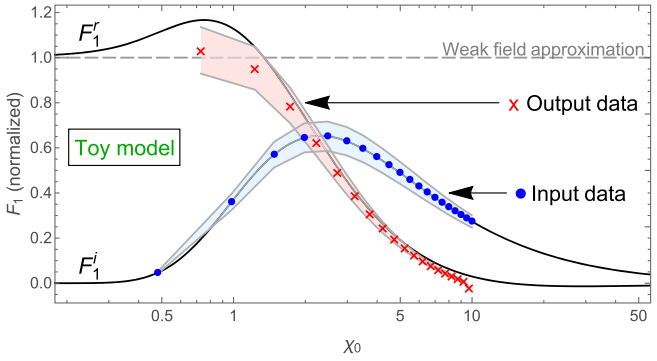

FIG. 1. A toy model. The real and imaginary parts of F_1 (solid curves) normalized to its weak-field limit, assuming monoenergetic, completely polarized photons propagating in a constant crossed field. (The curves for F_2 are similar up to an overall constant scale factor.) The blue/filled circles sample the imaginary part, representing the measured pair yield, which is input data for the numerical Hilbert transform. The red crosses are the output data $\overline{F_1^r}$, which estimates the real part F_1^r. The bands model a 10% (systematic) uncertainty in the pair yield measurement. The leading-order Heisenberg-Euler approximation to F_1 yields the horizontal dashed line, included to emphasize that we work beyond the weak-field regime.

from the transform—however, their contribution is small. We also see that if there is an uncertainty in the measured pair yield on the order of 10%, a comparable level of uncertainty is transferred to the prediction of the vacuum polarization effect. The curves in Fig. 1 are normalized to their weak-field limit (which is purely real since pair creation is suppressed in the limit). In fact the weak-field approximations to F are straight lines, hence Fig. 1 emphasizes that, both here and below, we go beyond the weak-field approximation.

IV. SETUP

To assess our scheme in a realistic case, we turn to a setup similar to the planned LUXE experiment [17], in which electron-positron pairs will be generated via the nonlinear Breit-Wheeler process. This will be achieved by colliding a 16.5 GeV monoenergetic beam of electrons with a fixed amorphous target to produce a source of bremsstrahlung photons that will collide with a weakly focused laser pulse. (More details about how an experimental error of 10% can be achieved are given in the LUXE Conceptual Design Report [17].) Here we consider how a minimal modification of this setup can allow for an indirect measurement of nonlinear vacuum birefringence. Instead of the amorphous target, we suggest using a thin-target diamond radiator, which produces partially polarized CB. The bremsstrahlung photons then collide at a fixed angle with a focused laser pulse, and the overlap with the focal spot provides natural collimation of the photons. A specific collimation is assumed in calculation of the CB spectrum; details of this, and how the yield for partially polarized photons is inverted to acquire the yield from photons in state $|j\rangle$, are given in Appendices B and C respectively. The scenario is sketched in Fig. 2. We now present three example results.

V. LEADING-ORDER VACUUM BIREFRINGENCE

The envisaged setup using CB photons colliding with a focused Gaussian laser pulse, combined with a Hilbert transform of the measured pair yield, allows us to infer the full amplitude for photon helicity flip using (3). Define the fraction $\mathsf{R} = 2\mathcal{M}^r_{\pm}/(\mathcal{M}^r_{11} + \mathcal{M}^r_{22})$ which corresponds, in the low-χ limit, to the ratio of flip to average no-flip amplitude. These are inferred from the experiment and Hilbert transform, which yields an estimate $\overline{\mathsf{R}}$ to be compared with the theoretical prediction R. This ratio is particularly convenient to investigate as it connects directly to vacuum birefringence, which is the macroscopic result of photon helicity flip. To see this we note that in the (low-energy) regime $\chi, \eta \ll 1$, pair creation is suppressed and the photon-scattering amplitudes are well approximated by the replacement $\mathcal{M}_{jj} \to \mathcal{M}^r_{jj}$ i.e. using just the real part. This allows one to describe vacuum polarization effects using a semiclassical approach, based upon a real "vacuum refractive index," $n_j = 1 + \delta n_j$ [26,35]. For photons with energy ω in polarization eigenstate $|j\rangle$, the leading-order weak-field Heisenberg-Euler result for δn_j is

$$\delta n_j = -\alpha m^2 \mathcal{M}^{rr}_{jj}/\omega^2 \simeq c_j \chi^2 m^2/(k^0)^2, \tag{6}$$

in which the well-known low-energy constants of QED are $c_j = \alpha(1 + 3j)/90\pi$. Photons in different polarization states thus experience different dispersion relations in the quantum vacuum, and, from (3), the helicity flip probability is supported on the difference of the refractive indices, which is birefringence. In the low-energy, low-χ regime, all volumetric factors entering $\overline{\mathsf{R}}$ cancel, giving the approximation $\mathsf{R} \approx \mathsf{R}^{(wf)}$ where

$$\mathsf{R}^{(wf)} = \frac{c_1 - c_2}{c_1 + c_2}. \tag{7}$$

For QED, $\mathsf{R}^{(wf)} = 3/11 \approx 0.273$. We calculate $\overline{\mathsf{R}}$ for our setup and compare with the exact value in Fig. 3. The larger the maximum value of χ_0 for which the pair yield is

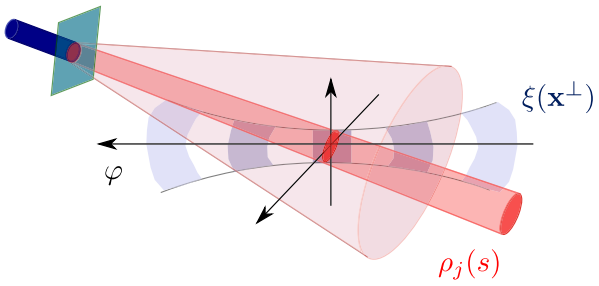

FIG. 2. A partially polarized source of coherent bremsstrahlung photons, $\rho_j(s)$ collides with a focused laser pulse with intensity parameter $\xi(\mathbf{x}^\perp)$ and the overlap with the focal spot provides a natural collimation.

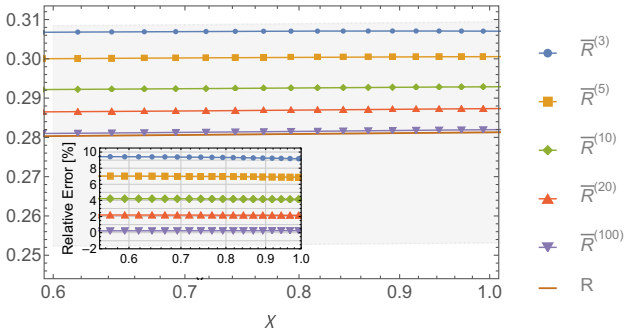

FIG. 3. Results for the birefringence measure $\overline{\mathsf{R}}$ in the "low-energy" region for the collision of photons generated via coherent bremsstrahlung with a focused laser pulse as described in the text. The results $\overline{\mathsf{R}}^{(\chi_{\max})}$ correspond to using measurements of the number of pairs for χ values up to $\chi_{\max}$, which are to be compared to the exact value, given by R. The gray region indicates $\pm 10\%$ of the true value, and the relative error to the true value of each curve is given in the inset.

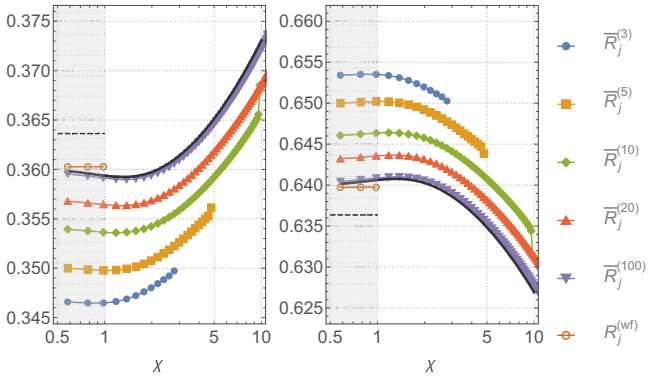

FIG. 4. Plot of $\overline{\mathsf{R}}_j$, the ratio of "no-flip" amplitude in state $|j\rangle$ to average "no-flip" amplitude, for $j = 1$ (left) and $j = 2$ (right). The solid black lines are the exact results. The curves with data points are example projections from Hilbert transforming the yield of pairs created by photons in the two polarization eigenstates. The low-energy region of $\chi < 1$ is shaded in gray and the low-energy approximation $\mathsf{R}_j^{(\mathrm{wf})}$ (the leading-order term in a weak-field expansion of the Heisenberg-Euler result) is also shown. The black dashed line corresponds to the coarse approximation of just using the low-energy constants, i.e. the idealized situation assuming photons completely polarized in an eigenstate, giving $\mathsf{R}_1 \approx 4/11 \approx 0.363$ and $\mathsf{R}_2 \approx 7/11 \approx 0.636$.

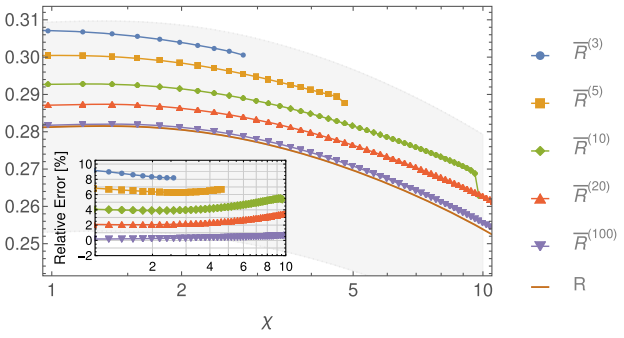

FIG. 5. The birefringence measure $\overline{\mathsf{R}}$ in the "high-energy" region for the collision of photons generated via coherent bremsstrahlung with a focused laser pulse as described in the text. When $\chi \gtrsim 1$, the perturbative, low-energy limit given by the leading-order Heisenberg-Euler result is no longer valid and instead, the result depends on all orders of interaction between the virtual pair and the background.

measured, the more accurate the prediction of vacuum birefringence. We find that for the range $0.5 < \chi_0 < 3$, the prediction is accurate to within 10%. By comparison, in stage 1 of the LUXE experiment, χ_0 can be varied up to around $\chi_0 = 4.5$ [17], which would improve the accuracy of the result. We note that the small-χ limit in Fig. 3 compares well with the theoretical approximation (7).

VI. DEVIATION FROM LOW-ENERGY SCALING

Pair creation from photons in a given polarization state relates directly to "no-flip" observables [see Eq. (2)] and to the corresponding vacuum refractive index along an eigenpolarization. Thus an advantage of our approach is that it gives us access to *both* of the individual low-energy constants of QED. This is in contrast to measuring vacuum birefringence directly, such as via the induced ellipticity in a linearly polarized probe, which is only sensitive to the difference of the refractive indices. (See also [36,37] for other approaches to the determination of the individual constants.) A second advantage is that we are sensitive to the changes in vacuum polarization effects which occur as one increases the strong-field parameter χ. To see this, we calculate $\overline{\mathsf{R}}_j = 2\overline{\mathcal{M}}^r_{jj}/(\overline{\mathcal{M}}^r_{11} + \overline{\mathcal{M}}^r_{22})$ for our considered setup. The results are presented in Fig. 4. We highlight, in the plot, the low-energy/weak-field approximations $\overline{\mathsf{R}}_j \sim c_j/(c_1 + c_2)$. We match these to a good approximation at low χ. Indeed the weak-field approximation would be a horizontal line on the plot; the deviation from this low-energy scaling, as we increase χ, is clearly visible in the plot.

VII. NONLINEAR (ALL-ORDER) VACUUM BIREFRINGENCE

When $\chi \ll 1$, vacuum birefringence cannot be described by the Heisenberg-Euler weak-field result. As χ is increased, the refractive indices reach a maximum, decrease, and even change sign [26,38,39]—none of which is captured by the weak-field approximation. One advantage of the method outlined here, of using the yield of pairs created by photons in different polarization eigenstates, is that it can be used when $\chi \ll 1$, in the regime of nonlinear vacuum birefringence where all orders of interaction between the virtual pair and the background must be taken into account. In fact, as χ increases, more pairs are created, so the method should in principle require less statistics, i.e. fewer collisions. In order to test the QED prediction of nonlinear vacuum birefringence, the same measure R can be used. As shown in Fig. 5, the dependence of R on χ at higher χ is very different compared to the weak-field, leading-order Heisenberg-Euler result, which would be a straight line. Similar levels of accuracy are achieved as for the weak-field case, depending on the range of χ that measurements can be performed over.

VIII. CONCLUSION

We have shown how photon-photon scattering effects in QED can be indirectly measured from experimental observation of pair production in intense laser fields. Complementary to direct searches for vacuum birefringence, our method avoids signal/noise problems associated with measuring signal photons in laser backgrounds, and it also works with linearly polarized laser light. Our methods give access to both vacuum refractive indices, not just the

difference. A requirement that the procedure be accurate is that the pair yield must be measured over a sufficiently broad range of χ. Being based, fundamentally, on unitarity and analyticity, our ideas can in principle be extended to other processes and to higher loops. Measurements of pair yield in a parameter regime where a significant fraction of pairs are "second generation" could potentially yield insight into the Ritus-Narozhny conjecture on the higher-loop behavior of strong-field QED at high χ [8,40]. We also note that for future direct searches of new physics using photon-photon scattering (e.g. signs of other particles "running in the loop"), a good understanding of the Standard Model signal will be essential, and our indirect measurement adds to the available methods by which this signal can be determined.

ACKNOWLEDGMENTS

B. K. thanks S. Boogert, L. Helary and G. Sarri for useful discussions and acknowledges support from the Deutsche Forschungsgemeinschaft (DFG, German Research Foundation) under Germany's Excellence Strategy—EXC 2121 "Quantum Universe"—390833306 and from the Engineering and Physical Sciences Research Council (EPSRC), Grant No. EP/S010319/1.

APPENDIX A: HILBERT TRANSFORM OF PAIR DATA

Denote the number of pairs measured with maximum photon strong-field parameter $\chi_0 = \xi_0\eta$ as $N_j(\chi_0)$, as defined in Eq. (C1), and the corresponding value of the function to Hilbert transform as $F^i(\chi_0) = N_j/\eta_e\xi_0^2$. Then supposing a set of M measurements $\{F_i(\chi_{0,1}), \ldots, F_i(\chi_{0,M})\}$ are made, one can perform a Hilbert transform using these points for an indirect "measurement," denoted $\overline{F^r}(\tilde{\chi}_0)$, $(\tilde{\chi}_0 \notin \{\chi_{0,1}, \ldots, \chi_{0,M}\})$ which encodes, e.g. the vacuum refractive indices. The Hilbert transform of a function $F^i(\chi)$ is

$$\mathcal{H}[F_i;\chi] = \frac{1}{\pi}\mathrm{PV}\int \mathrm{d}\chi' \frac{F^i(\chi')}{\chi' - \chi}, \tag{A1}$$

and here, $\overline{F^r}(\tilde{\chi}_0) = \mathcal{H}[F^i;\tilde{\chi}_0]$. Since physical values of the χ parameter always fulfill $\chi \geq 0$, the integral must be analytically continued to negative values of χ. This is achieved using the prescription

$$F_i(\chi) \coloneqq \mathrm{sgn}(\chi)F_i(|\chi|), \tag{A2}$$

which allows us to use all measured data points twice in the same numerical Hilbert transform. The total set of points used is

$$\{F_i(-\chi_{0,M}), \cdots F_i(-\chi_{0,1}), F_i(\chi_{0,1}), \ldots, F_i(\chi_{0,M})\}.$$

The principal value is taken numerically by splitting the data points into a lower set: $S_< = \{F_i(-\chi_{e,M}), \cdots F_i(\chi_{e,j})\}$ and an upper set: $S_> = \{F_i(\chi_{e,j+1}), \ldots, F_i(\chi_{e,M})\}$, and integrating over both sets independently, after which the values are combined: $\mathrm{PV}\int \mathrm{d}\chi' = \int_{S_<} \mathrm{d}\chi' + \int_{S_>} \mathrm{d}\chi'$. A suitable set of $\tilde{\chi}_0$ values on which to evaluate the Hilbert transform is given by the midpoints of the χ_0 values of the measurements, so $\{\tilde{\chi}_{0,1}, \ldots, \tilde{\chi}_{0,M-1}\}$ where $\tilde{\chi}_{0,j} = (\chi_{0,j} + \chi_{0,j+1})/2$. The $\chi_{0,j}$ values are assumed to be uniformly distributed, which helps to prevent spurious effects from arising in the numerical Hilbert transform.

The accuracy of the transform, in comparison to the target function, can be further increased by extrapolating beyond the range of measured values, assuming an asymptotic scaling. This is achieved by taking the measured value at maximum χ, i.e. $F_i(\chi_{0,M})$ and assuming that for larger χ_0, F_i follows the asymptotic behavior $F_i(\chi_0) \sim \chi_0^{-4/3}$ implied by the (locally) constant crossed field approximation. [The probability $\mathsf{P}^{\mathrm{ccf}}$ for pair creation at large χ scales as $\mathsf{P}^{\mathrm{ccf}} \sim \chi^{2/3}/\eta$ [41], and $F_i(\chi) = \mathsf{P}^{\mathrm{ccf}}/\eta\xi^2$]. In the text, we applied this asymptotic scaling from $\chi_{0,M}$ to $\chi_0 = 10^3$.

APPENDIX B: COHERENT BREMSSTRAHLUNG

Here we describe the model used for bremsstrahlung. As pointed out in the main text, the energy spectrum and polarization degree of coherent bremsstrahlung depend on the extent of the collimation. Here we assume an "effective collimation" to be provided by the position and dimension of the laser focal spot that the bremsstrahlung collides with. Specifically, the coherent bremsstrahlung spectrum was calculated for collision with a laser pulse of waist $w_0 = 25$ μm and a focal spot at a distance of 3 m from the target. (These figures correspond to $\xi = 1$ in stage 0 of the LUXE experiment [17].) For calculations involving bremsstrahlung at different intensity parameters ξ', we scale the number of photons by the ratio of areas, i.e. $(\xi/\xi')^2$. This is an approximation because it assumes the same bremsstrahlung spectral content, even though the collimation angle is reduced.

Although our main interest is in coherent bremsstrahlung, we also calculate the distribution of (collimated) incoherent thin-target bremsstrahlung $\rho^{(b)}$ from an amorphous target, as a test case to compare our analytical approach with the results of full numerical simulations in [17]. The $\rho^{(b)}$ distribution is modelled as

$$\rho^{(b)} = N_e\frac{X}{X_0}\left[1 - \exp\left(-\frac{\psi_{\mathrm{col.}}^2}{2\sigma_{\mathrm{tot.}}^2}\right)\right]\left[\frac{4}{3s}(1-s) + s\right], \tag{B1}$$

where N_e is the number of electrons, X_0 the radiation length, X the target thickness, $\psi_{\mathrm{col.}}$ the effective collimation angle and $\sigma_{\mathrm{tot.}}$ the total angular divergence of the bremsstrahlung photon pulse. The angular divergence of the bremsstrahlung

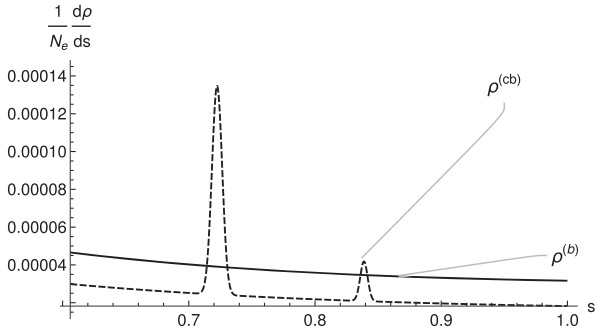

FIG. 6. A comparison of the energy spectrum of the incoherent bremstrahlung photons from an amorphous target $\rho^{(b)}$, and the spectrum of coherent bremsstrahlung photons $\rho^{(cb)}$ from a diamond CVD target.

photons can be written $\sigma_{\text{tot.}} = (\sigma_e^2 + \sigma_0^2)^{1/2}$, where σ_e is the electron beam angular divergence due to multiple scattering in the target, and σ_0 is the intrinsic divergence of bremsstrahlung photons. The intrinsic divergence of the bremsstrahlung photons is given by $\sigma_0 = 0.52/\gamma_e$, where γ_e is the Lorentz gamma factor of the initial 16.5 GeV electrons, which we assume does not depend on the initial photon energy.

In the calculation of the CB distribution, $\rho^{(cb)}$, we have chosen the orientation of the diamond target such as to provide the first CB peak at around 12 GeV (corresponding to a lightfront fraction of $s = 0.725$). This contribution arises from the single reciprocal lattice vector (2, 2, 0). The collimation factor of the coherent bremsstrahlung was assumed to have the same form as the incoherent bremsstrahlung distribution [first square bracket in Eq. (B1)]. The coherent component of bremsstrahlung was calculated taking into account the electron beam divergence σ_e and the collimation angle $\psi_{\text{col.}}$ using the standard method [42,43].

From a full calculation of CB from a diamond target with thickness $X = 0.005\,X_0$ ($X_0 = 0.6$ mm), we find the first two peaks of the CB distribution can be approximated as

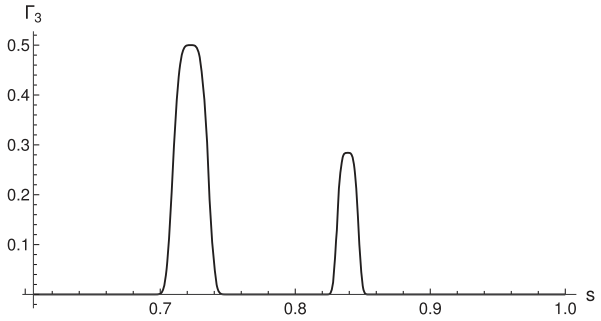

FIG. 7. The Stokes parameter Γ_3 of the CB photons can be as large as 0.5.

$$\rho^{(cb)} = N_e C_X \left[\frac{C_s^{(0)}}{s}(1-s) + C_s^{(1)} s + \sum_{i=1}^{2} A^{(i)} \mathrm{e}^{-\frac{(s-s_i)^2}{2\sigma_i^2}}\right] \quad \text{(B2)}$$

where $C_X = 0.000276$, $C_s^{(0)} = 0.105$, $C_s^{(1)} = 0.066$, $A^{(1)} = 0.4$, $A^{(2)} = 0.076$. $\sigma_1 = 0.004$, $\sigma_2 = 0.003$ with CB peaks at $s_1 = 0.72$ $s_2 = 0.84$ corresponding to 11.92 and 13.84 GeV respectively. Due to a "hard" collimation ($\psi_{\text{col.}} \ll 1/\gamma$) the spectral width of the CB peaks becomes especially narrow, even though the conventional condition $\psi_{\text{col.}} > \sigma_e$ is not fulfilled. The spectra $\rho^{(b)}$ and $\rho^{(cb)}$ are plotted and compared in Fig. 6.

The polarization of the CB peaks was calculated and the following parametrization found:

$$\Gamma_3 = A_1^\Gamma \exp\left[-\frac{(s-s_1)^4}{2(\sigma_1^\Gamma)^4}\right] + A_2^\Gamma \exp\left[-\frac{(s-s_2)^4}{2(\sigma_2^\Gamma)^4}\right], \quad \text{(B3)}$$

where $A_1^\Gamma = 0.5$, $A_2^\Gamma = 0.284$, $\sigma_1^\Gamma = 0.012$, $\sigma_2^\Gamma = 0.0073$, where the Stokes parameter Γ_3 remains practically constant in the narrow range near the CB peaks ($\Gamma_3 = A_n^\Gamma$, for $n = 1, 2$) and vanishes outside. The Stokes parameter is the asymmetry in polarizations, which we write as

$$\Gamma_3 = \frac{\rho_1^{(cb)} - \rho_2^{(cb)}}{\rho_1^{(cb)} + \rho_2^{(cb)}}. \quad \text{(B4)}$$

In the setup we consider, the Stokes parameters are defined in the coordinate system which aligns with the crystallographic plane (2, 2, 0), to an accuracy of $1/\gamma$, where γ is the Lorentz factor of the electrons generating the coherent bremsstrahlung. (For 16.5 GeV electrons, $\gamma^{-1} \approx 3 \times 10^{-5}$.)

In Appendix C, a test of the distributions in Eqs. (B1) and (B2) is made, in which the yield of pairs is calculated for LUXE parameters and compared to the simulation results. We find good qualitative agreement and approximate quantitative agreement between the results for the full simulational approach, and the analytical results presented here.

APPENDIX C: CALCULATION OF NUMBER OF PAIRS

The number of pairs is calculated using the formula

$$N_j = \frac{2\alpha}{\eta} \int \mathrm{d}^2\mathbf{x}^\perp \int \mathrm{d}\varphi \int_0^1 \mathrm{d}s\, \rho_j(s) \mathcal{M}_{jj}^i[\xi(\varphi, \mathbf{x}^\perp), s]. \quad \text{(C1)}$$

We model the focused pulse using the infinite Rayleigh length approximation [44,45] as $\xi(\varphi, \mathbf{x}^\perp) = \xi_0 f(\varphi, \mathbf{x}^\perp)$, where

$$f(\varphi, \mathbf{x}^\perp) = \mathrm{e}^{-\frac{|\mathbf{x}^\perp|^2}{w_0^2}} g(\varphi) \cos(\varphi),$$

with $g(\varphi) = \partial[\sin^2(\varphi/2N)]/\partial\varphi$ for $0 < \varphi < 2\pi N$ and $N = 16$ is the number of cycles, $g(\varphi) = 0$ otherwise and w_0 the Gaussian waist.

In Fig. 8, we compare the prediction of Eq. (C1) using parameters of the LUXE experiment with the results of [17], generated by using the code PTARMIGAN [30] to simulate the creation of pairs at the interaction point from bremsstrahlung calculated by GEANT4 [46]. To compare the results in [17], which are for a circularly-polarized pulse, to the current work, which uses a linearly polarized pulse, we multiply them by a factor of 2. (This assumes that at the same ξ, the area of overlap between the bremsstrahlung and laser pulse can be doubled, but does not take into account any effect due to a different collimation angle.) The collimation of the bremsstrahlung and CB spectra described in Appendix B used parameters in stage 0 of LUXE; in order to compare with stage 1, we multiply these results by a factor equal to the ratio of powers of stage 0 and stage 1, i.e. 35/4, to take into account a larger interaction area at constant ξ. (Since our aim is to verify that the order of magnitude of pairs is correct, rather than perform a high-precision comparison, also here, we do not recalculate the bremsstrahlung spectra for a new collimation angle.) As can be seen in Fig. 8, we find good agreement with the order of magnitude of the simulated results and our theory calculations.

In order to calculate the number of pairs from the partially polarized coherent bremsstrahlung, we must combine results from the previous and current sections. We consider two configurations of the CB target: "$\parallel$," where the dominant CB polarization direction is parallel to the laser polarization and "$\perp$," where the dominant CB polarization direction is perpendicular to the laser polarization (both definitions assuming a head-on collision of photons with the laser pulse). The differential number of pairs produced in the two configurations is $N^{\parallel,\perp} = \int(\mathrm{d}N^{\parallel,\perp}/\mathrm{d}s)\mathrm{d}s$, where

$$\begin{aligned}\frac{\mathrm{d}N^{\parallel}}{\mathrm{d}s} &= \mathcal{P}(s)\frac{\mathrm{d}N_1}{\mathrm{d}s} + [1-\mathcal{P}(s)]\frac{\mathrm{d}N_2}{\mathrm{d}s}\\ \frac{\mathrm{d}N^{\perp}}{ds} &= [1-\mathcal{P}(s)]\frac{\mathrm{d}N_1}{\mathrm{d}s} + \mathcal{P}(s)\frac{\mathrm{d}N_2}{\mathrm{d}s}\end{aligned} \tag{C2}$$

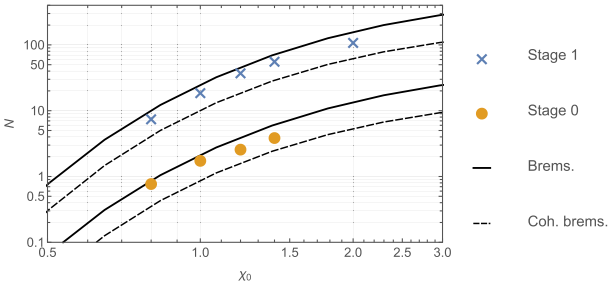

FIG. 8. Plot of the number of pairs calculated by Eq. (C1) using the bremsstrahlung photon distribution, $\rho^{(b)}$ from Eq. (B1) and (unpolarized) coherent bremsstrahlung, $\rho^{(cb)}$ from Eq. (B2), compared to the simulation results from [17] for the stage 0 and stage 1 parameters of LUXE.

where $\mathcal{P}(s) = [1 + \Gamma_3(s)]/2$, and $\Gamma_3(s)$ is defined in Eq. (B3) above: the function $\mathcal{P}(s)$ then denotes the fraction of CB photons with energy fraction s in polarization state $|1\rangle$. It is then assumed that although the dependency on the photon energy of the created pairs may not be measurable in fine resolution, at least the pairs created by the first CB peak at $s = s_1$ can be identified, using e.g. a gamma spectrometer concept such as described in [47]. Then the inversion to find the number of pairs created by photons in eigenstates $|j\rangle$, can be written as

$$\begin{aligned}N_1 &= \frac{\mathbb{P}N^{\parallel} - (1-\mathbb{P})N^{\perp}}{2\mathbb{P}-1}\\ N_2 &= \frac{\mathbb{P}N^{\perp} - (1-\mathbb{P})N^{\parallel}}{2\mathbb{P}-1},\end{aligned} \tag{C3}$$

where $\mathbb{P}$ is a constant polarization degree that represents the polarization of photons in the CB peak. We determined $\mathbb{P}$ by calculating the mean polarization contributing value to pair creation. For the peak between 11.92 ± 0.25 GeV corresponding to $0.707 < s < 0.738$, this was $\mathbb{P} = 0.722$ (recall from Fig. 7 that there is a plateau of $\Gamma_3 = 0.5$ at the center of the peak, equivalently: $\mathcal{P} = 0.75$). That this is a physically relevant choice is evidenced by the good agreement in the low-χ limit of the results for predicted birefringence in Fig. 3, with the low-χ limit of the helicity flipping amplitude.

[1] O. Halpern, Phys. Rev. **44**, 855 (1933).
[2] M. Aaboud *et al.* (ATLAS Collaboration), Nat. Phys. **13**, 852 (2017).
[3] G. Aad *et al.* (ATLAS Collaboration), Phys. Rev. Lett. **123**, 052001 (2019).
[4] A. M. Sirunyan *et al.* (CMS Collaboration), Phys. Lett. B **797**, 134826 (2019).
[5] G. Jarlskog, L. Joensson, S. Pruenster, H. D. Schulz, H. J. Willutzki, and G. G. Winter, Phys. Rev. D **8**, 3813 (1973).

[6] M. Schumacher, I. Borchert, F. Smend, and P. Rullhusen, Phys. Lett. **59B**, 134 (1975).
[7] B. King and T. Heinzl, High Power Laser Sci. Eng. **4**, e5 (2016).
[8] A. Fedotov, A. Ilderton, F. Karbstein, B. King, D. Seipt, H. Taya, and G. Torgrimsson, arXiv:2203.00019.
[9] T. Heinzl, B. Liesfeld, K.-U. Amthor, H. Schwoerer, R. Sauerbrey, and A. Wipf, Opt. Commun. **267**, 318 (2006).
[10] A. Di Piazza, K. Z. Hatsagortsyan, and C. H. Keitel, Phys. Rev. Lett. **97**, 083603 (2006).
[11] H.-P. Schlenvoigt, T. Heinzl, U. Schramm, T. E. Cowan, and R. Sauerbrey, Phys. Scr. **91**, 023010 (2016).
[12] F. Karbstein, H. Gies, M. Reuter, and M. Zepf, Phys. Rev. D **92**, 071301 (2015).
[13] A. Ilderton and M. Marklund, J. Plasma Phys. **82**, 655820201 (2016).
[14] B. King and N. Elkina, Phys. Rev. A **94**, 062102 (2016).
[15] S. Bragin, S. Meuren, C. H. Keitel, and A. Di Piazza, Phys. Rev. Lett. **119**, 250403 (2017).
[16] V. I. Ritus, J. Sov. Laser Res. **6**, 497 (1985).
[17] H. Abramowicz *et al.*, Eur. Phys. J. Special Topics **230**, 2445 (2021).
[18] Z. Chen, S. Meuren, E. Gerstmayr, V. Yakimenko, P. H. Bucksbaum, and D. A. Reis, in *Optica High-Brightness Sources and Light-Driven Interactions Congress, 2022* (Optica Publishing Group, Washington, DC, 2022), p. HF4B.6.
[19] D. L. Burke *et al.*, Phys. Rev. Lett. **79**, 1626 (1997).
[20] C. Bamber *et al.*, Phys. Rev. D **60**, 092004 (1999).
[21] J. Adam *et al.* (STAR Collaboration), Phys. Rev. Lett. **127**, 052302 (2021).
[22] R. P. Mignani, V. Testa, D. G. Caniulef, R. Taverna, R. Turolla, S. Zane, and K. Wu, Mon. Not. R. Astron. Soc. **465**, 492 (2017).
[23] L. M. Capparelli, A. Damiano, L. Maiani, and A. D. Polosa, Eur. Phys. J. C **77**, 754 (2017).
[24] S. Adhikari *et al.* (GlueX Collaboration), Nucl. Instrum. Methods Phys. Res., Sect. A **987**, 164807 (2021).
[25] D. C. Hutchings, M. Sheik-Bahae, D. J. Hagan, and E. W. van Stryland, Opt. Quantum Electron. **24**, 1 (1992).
[26] J. S. Toll, Ph.D. thesis, Princeton University, 1952.
[27] A. Di Piazza, M. Tamburini, S. Meuren, and C. H. Keitel, Phys. Rev. A **98**, 012134 (2018).
[28] A. Ilderton, B. King, and D. Seipt, Phys. Rev. A **99**, 042121 (2019).
[29] B. King, Phys. Rev. A **101**, 042508 (2020).
[30] T. G. Blackburn and B. King, Eur. Phys. J. C **82**, 44 (2022).
[31] T. Heinzl and O. Schroeder, J. Phys. A **39**, 11623 (2006).
[32] A. Di Piazza, Phys. Rev. Lett. **117**, 213201 (2016).
[33] E. G. Gelfer, A. M. Fedotov, A. A. Mironov, and S. Weber, Phys. Rev. D **106**, 056013 (2022).
[34] V. N. Baier, A. I. Milshtein, and V. M. Strakhovenko, Sov. Phys. JETP **42**, 961 (1975).
[35] R. Baier and P. Breitenlohner, Nuovo Cimento B **47**, 117 (1967).
[36] M. Fouché, R. Battesti, and C. Rizzo, Phys. Rev. D **93**, 093020 (2016); **95**, 099902(E) (2017).
[37] F. Karbstein, D. Ullmann, E. A. Mosman, and M. Zepf, Phys. Rev. Lett. **129**, 061802 (2022).
[38] G. M. Shore, Nucl. Phys. **B778**, 219 (2007).
[39] V. Dinu, T. Heinzl, and A. Ilderton, Phys. Rev. D **86**, 085037 (2012).
[40] A. M. Fedotov, J. Phys. Conf. Ser. **826**, 012027 (2017).
[41] A. I. Nikishov and V. I. Ritus, Sov. Phys. JETP **19**, 529 (1964).
[42] D. Lohmann, J. Peise, J. Ahrens, I. Anthony, H.-J. Arends, R. Beck, R. Crawford, A. Hünger, K. Kaiser, J. Kellie *et al.*, Nucl. Instrum. Methods Phys. Res., Sect. A **343**, 494 (1994).
[43] B. Kalinin, G. Naumenko, A. Potylitsin, V. Verzilov, I. Vnukov, K. Yoshida, K. Goto, I. Endo, T. Isshiki, T. Kondo *et al.*, Nucl. Instrum. Methods Phys. Res., Sect. B **145**, 209 (1998).
[44] H. Gies, F. Karbstein, and C. Kohlfürst, Phys. Rev. D **97**, 036022 (2018).
[45] B. King, H. Hu, and B. Shen, Phys. Rev. A **98**, 023817 (2018).
[46] J. Allison *et al.*, Nucl. Instrum. Methods Phys. Res., Sect. A **835**, 186 (2016).
[47] K. Fleck, N. Cavanagh, and G. Sarri, Sci. Rep. **10**, 9894 (2020).